Spectral dimensions of hierarchical scale-free networks with weighted shortcuts

S. Hwang,[1] C.-K. Yun,[1] D.-S. Lee,[2,*] B. Kahng,[1,3,†] and D. Kim[1,3]
[1]*Department of Physics and Astronomy, Seoul National University, Seoul 151-747, Korea*
[2]*Department of Natural Medical Sciences and Department of Physics, Inha University, Incheon 402-751, Korea*
[3]*School of Physics, Korea Institute for Advanced Study, Seoul 130-722, Korea*
(Received 17 June 2010; revised manuscript received 7 September 2010; published 12 November 2010)

Spectral dimensions have been widely used to understand transport properties on regular and fractal lattices. However, they have received little attention with regard to complex networks such as scale-free and small-world networks. Here, we study the spectral dimension and the return-to-origin probability of random walks on hierarchical scale-free networks, which can be either fractal or nonfractal depending on the weight of the shortcuts. Applying the renormalization-group (RG) approach to a Gaussian model, we obtain the exact spectral dimension. While the spectral dimension varies between 1 and 2 for the fractal case, it remains at 2, independent of the variation in the network structure, for the nonfractal case. The crossover behavior between the two cases is studied by carrying out the RG flow analysis. The analytical results are confirmed by simulation results and their implications for the architecture of complex systems are discussed.

DOI: 10.1103/PhysRevE.82.056110 PACS number(s): 89.75.Hc, 89.75.Fb, 05.40.−a, 05.10.Cc

I. INTRODUCTION

The problem of random walks (RWs) on complex networks has attracted much attention as a model for studying diffusion processes on complex systems such as fad or disease spreading over social networks, data packet transport over the Internet, and data mining on the Web [1–6]. These important applications have led to extensive studies of the problem [7–15], but it still remains unclear how RW properties depend on the network structure. In this study, we investigate the effect of shortcut links on RW motion. Shortcuts may be classified into two types: long-range shortcuts, which are utilized in a skeleton or in superhighways, and local shortcuts, which are complementary to the skeleton or local roads [16–18]. It was recently shown systematically [19] that long-range shortcuts can change the type of a network from fractal to nonfractal. The fractal (nonfractal) network is the one in which the mean separation between two nodes scales algebraically (logarithmically) with the system size. We are particularly interested in how RW properties change as long-range shortcuts are added, thereby changing the network from a fractal to a nonfractal network.

We used a Gaussian model, which is useful for studying RW problems analytically [20], to understand the RW motion on hierarchical scale-free networks [21–24]. In this artificial network, we can control the strength distribution and the link weight of the shortcuts. We consider RWs on this hierarchical network and obtain the exact solution of the return-to-origin (RTO) probability by applying the renormalization-group (RG) approach to the Gaussian model. The RTO probability is related to the free energy of the Gaussian model and the spectral density function of the Laplacian matrix, all of which are characterized by the spectral dimension d_s [1,20]. The hierarchical network is recursively organized, so that one can analytically obtain the spectral density function by using the decimation method of the RG transformation. We find that when the network structure is a fractal, the spectral dimension d_s varies in the range $1<d_s\leq 2$; however, for nonfractal networks, it is fixed at $d_s=2$. These analytical results are confirmed by numerical simulations. Moreover, we perform the numerical simulations of RWs on various real-world networks and check the relationship between the network fractality and the spectral dimension.

The paper is organized as follows. In Sec. II, the hierarchical network model and the formalism to derive the spectral density function of the Laplacian matrix from the Gaussian model are briefly introduced along with their relation to the RTO probability of RWs. In Sec. III, we apply the RG approach to the Gaussian model and obtain the spectral density function explicitly. In Sec. IV, numerical results of the RTO probability are presented and compared with the analytical solutions. We summarize our findings and discuss their implications in Sec. V.

II. MODEL AND FORMALISM

The network we use in the study is a modified version of an existing hierarchical network model [21–24], in which shortcuts are assigned weights. We call this modified model the *weighted flower* (WF) network. The WF network contains two types of links, types I and II, which evolve differently. The WF network is constructed iteratively as follows. We start from a single type-I link between two nodes, which is the zeroth generation. At the next generation, two chains are added between the two nodes of the type-I link. On one chain, $u-1$ nodes are located and thereby u links are placed. On the other chain, $v-1$ nodes are located and thereby v links are placed. These $u+v$ links are assigned as type-I links, and the type of seed link is changed to type II. These steps—adding nodes and links and assigning link types—are carried out for every generation. Every link is assigned a weight: 1 for each type-I link and p for each type-II link. The link weights will be used as the transition rate of random walkers (RWers). The growth of the WF network with $u=2$

*deoksun.lee@inha.ac.kr
†bkahng@snu.ac.kr

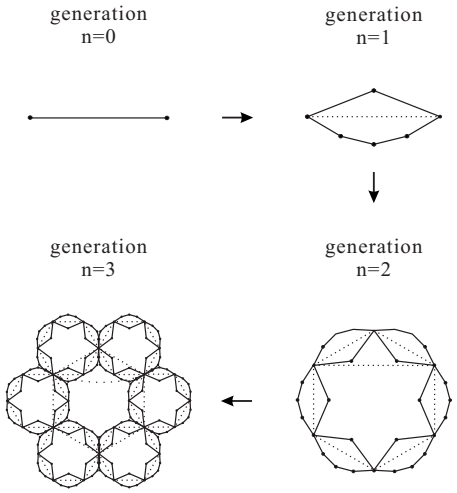

FIG. 1. Weighted flower (WF) network. The WF network with $u=2$ and $v=4$ is constructed from $n=0$th generation to $n=3$rd generation. Type-I links (solid line) and type-II links (dotted line) have link weights 1 and p, respectively.

and $v=4$ is depicted in Fig. 1. Throughout this paper, we will be considering the case of $u\geq 2$ and $v\geq 2$. If $u=1$ $(v=1)$, the upper (lower) chain is one link, which is essentially a type-II link, and the WF network becomes a nonfractal one [23]. For $u\geq 2$ and $v\geq 2$, the type-II links play the role of shortcuts in the system and the parameter p represents the transition rate across a type-II link. We would like to point out that in the previous model of the hierarchical network [21–24], the parameter p was used as the occupation probability of the type-II links; but here, it is used as the weight of the type-II links. Thus, the two network models are equivalent if $p=0$ or $p=1$. Otherwise, they are different.

The link weights of the WF network of the nth generation are represented in a symmetric matrix form

$$W_{\ell q}=\begin{cases}1, & (\ell q)\in E_n^{(\mathrm{I})}\\ p, & (\ell q)\in E_n^{(\mathrm{II})}\\ 0, & \text{otherwise},\end{cases} \tag{1}$$

where $E_n^{(\mathrm{I})}$ and $E_n^{(\mathrm{II})}$ denote the sets of type-I and type-II links of the nth generation, respectively, and (ℓq) represents the link connecting nodes ℓ and q. The basic structural properties of the WF networks can be obtained analytically [22–24] and are summarized in Table I. Here, we define the strength s_ℓ of node ℓ as $s_\ell=\Sigma_q W_{q\ell}$. In weighted networks, the notion of the shortest path is different from the path with the minimal number of hops between two nodes as defined in the binary network. We define an optimal path as the path over which the sum of the costs becomes minimal, where the cost of a link (ℓ,q) is $c_{\ell q}=1/W_{\ell q}$. We define the distance between two nodes as the sum of the costs over the optimal path between them [25]. While the degree exponent γ_k and the strength exponent γ_s in Table I depend only on u and v, the mean distance between nodes depends on the weight p. When $p=0$, the type-II links are not considered in determining the minimum-cost paths. Then, the mean distance D between nodes in the WF networks is related to the total number of nodes as [22–24]

TABLE I. Basic properties of the WF network of nth generation. Here, ℓ is the node index and n_ℓ denotes the birth generation of node ℓ. The degree of a node denotes the number of links connected to the node, and the strength of a node is defined as the sum of the weights of connected links.

Number of type-I links	$L_n^{(\mathrm{I})}=(u+v)^n$
Number of type-II links	$L_n^{(\mathrm{II})}=\frac{(u+v)^n-1}{u+v-1}$
Number of nodes	$N_n=\frac{u+v-2}{u+v-1}(u+v)^n+\frac{u+v}{u+v-1}$
Node degree	$k_\ell=2^{n-n_\ell+2}-2$
Node strength	$s_\ell=(1+p)2^{n-n_\ell+1}-2p$
Degree distribution	$p(k)\sim k^{-\gamma_k}$ with $\gamma_k=1+\frac{\ln(u+v)}{\ln 2}$
Strength distribution	$p(s)\sim s^{-\gamma_s}$ with $\gamma_s=1+\frac{\ln(u+v)}{\ln 2}$

$$D\sim N^{1/d_f} \quad \text{with} \quad d_f=\frac{\ln(u+v)}{\ln(\min\{u,v\})}. \tag{2}$$

Here, d_f is the fractal dimension [26] of the WF networks with $p=0$. When $0<p\leq 1$, shortcuts may participate in the minimum-cost paths and the mean distance is logarithmically proportional to the number of nodes [22,27]

$$D\sim \ln N. \tag{3}$$

Let us consider a RWer located initially at node ℓ_0 and going around in the network with the transition probability $W_{\ell q}/\Sigma_{\ell'}W_{\ell' q}$ from node q to ℓ. Then, the probability $P_{\ell\ell_0}(t)$ of finding the RWer at node ℓ after time t is given by $P_{\ell\ell_0}(t)=[(I-L)^t]_{\ell\ell_0}$, where I is the identity matrix and L is the Laplacian matrix defined as $L_{\ell q}=\delta_{\ell q}-W_{\ell q}/s_q$ with node strength $s_q=\Sigma_\ell W_{\ell q}$.

The RTO probability $P_o(t)=N^{-1}\Sigma_\ell P_{\ell\ell}(t)$ is determined by the eigenvalues μ_i $(i=0,1,2,\ldots,N-1)$ of the Laplacian matrix L as

$$\begin{aligned}P_o(t)&=\frac{1}{N}\mathrm{Tr}(I-L)^t\\&=\frac{1}{N}\sum_{i=0}^{N-1}(1-\mu_i)^t\sim\int_0^\infty d\mu\rho(\mu)e^{-\mu t}+(-1)^t\\&\quad\times\int_0^\infty d\tilde{\mu}\rho(2-\tilde{\mu})e^{-\tilde{\mu}t},\end{aligned} \tag{4}$$

where we introduce the spectral density function $\rho(\mu)\equiv N^{-1}\Sigma_{i=0}^{N-1}\delta(\mu-\mu_i)$ in the thermodynamic limit $N\to\infty$ [28]. For large t, the term $(1-\mu_i)^t$ in Eq. (4) is dominant, as $\mu_i\to 0$ and $\mu_i\to 2$. The contribution from $\mu_i\simeq 2$, however, cannot be larger than that from $\mu_i\simeq 0$ because $P_o(t)\geq 0$, but can cause an oscillatory behavior in $P_o(t)$ depending on whether t is even or odd. For example, in d-dimensional regular lattices, the eigenvalues are symmetrically distributed about $\mu=1$, and $\rho(\mu)=\rho(2-\mu)\sim\mu^{d/2-1}$ for small μ. Thus, it follows from Eq. (4) that $P_o(t)\sim t^{-d/2}$ when t is even, and $P_o(t)=0$ when t is odd.

For fractal lattices, the spectral density function and the RTO probability are characterized by the spectral dimension d_s as [2]

$$\rho(\mu) \sim \mu^{d_s/2-1} \quad \text{for} \quad \mu \to 0,$$

$$P_o(t) \sim t^{-d_s/2} \quad \text{for} \quad t \to \infty. \tag{5}$$

We use these formulas in further discussions later.

The mean first passage time T between two nodes is related to the eigenvalues of the Laplacian matrix via $T=2\Sigma_i \mu_i^{-1}$ [29], which is scaled with system size N as $T \sim N^{2/d_s}$ for $d_s<2$ and $T \sim N$ for $d_s>2$ [11]. For the fractal WF network ($u \geq 2$, $v \geq 2$) with $p=0$ in the nth generation, it was shown that $T \sim (uv)^n \sim N^{\ln(uv)/\ln(u+v)}$ based on the scaling behavior of the mean first passage time between two hub nodes [23]. Thus, $d_s=2\ln(u+v)/\ln(uv)$. On the other hand, for nonfractal WF networks, only the case of $(u,v)=(1,2)$ and $p=0$ has been studied [11,14,23]. Thus, to clarify how the spectral dimension is differentiated between fractal and nonfractal networks, it is essential to study a broader class of nonfractal networks. Motivated by these previous studies, we examined the spectral dimension of the hierarchical network as it crosses over from a fractal to a nonfractal one by varying the parameter p in the range $0 \leq p \leq 1$.

The Gaussian model is useful for studying the spectral density of the underlying network. The Hamiltonian of the Gaussian model is

$$\mathcal{H}_G = \frac{1}{2}\sum_{\ell,q} W_{\ell q}(\phi_\ell - \phi_q)^2 = \sum_{\ell,q} L'_{\ell q}\phi_\ell \phi_q, \tag{6}$$

where ϕ_ℓ is the spin variable at node ℓ, $W_{\ell q}$ is the interaction strength or the link weight between nodes ℓ and q, and $L'_{\ell q}=s_\ell \delta_{\ell,q}-W_{\ell q}$ [30]. The Laplacian matrices L in Eq. (4) and L' in Eq. (6) can have different eigenvalues in heterogeneous networks where the node strength s_ℓ is different from node to node. Each spin variable ϕ_ℓ takes a real value between $-\infty$ and ∞ with weight $\exp(-\eta_\ell \phi_\ell^2)$, and the partition function is given by

$$Z_G \equiv \int \mathcal{D}\phi \exp\left[-\sum_\ell \eta_\ell \phi_\ell^2 - \sum_{\ell,q} L'_{\ell q}\phi_\ell \phi_q\right], \tag{7}$$

where $\mathcal{D}\phi=\Pi_{\ell=1}^N d\phi_\ell$. The partition function Z_G and its free energy $f_G=-N^{-1}\ln Z_G$ are singular when one of the η_ℓ's is equal to one of the eigenvalues of L'. If we introduce a parameter μ such that $\eta_\ell=-i\mu s_\ell$ and multiply L' by i, where the imaginary number i is needed to make the integral converge, the partition function in Eq. (7) is represented by

$$\begin{aligned} Z(\mu) &= \int \mathcal{D}\phi \exp\left[i\sum_\ell \mu s_\ell \phi_\ell^2 - i\sum_{\ell,q} L'_{\ell q}\phi_\ell \phi_q\right] \\ &= \int \mathcal{D}\phi \exp\left[i\mu\sum_\ell \phi_\ell^2 - i\sum_{\ell,q} \tilde{L}_{\ell q}\phi_\ell \phi_q\right] \\ &= \sqrt{\frac{(i\pi)^N}{\prod_\ell (\mu-\mu_\ell)}}, \end{aligned} \tag{8}$$

where we rescale ϕ_ℓ with $\sqrt{s_\ell}$ and drop the constant $\Pi_\ell 1/\sqrt{s_\ell}$ in the second line. The matrix $\tilde{L}$ defined as $\tilde{L}_{\ell q}=\delta_{\ell,q}-W_{\ell q}/\sqrt{s_\ell s_q}$ is obtained by a similarity transformation from L (see Appendix A). Thus, L and $\tilde{L}$ have the same eigenvalues $\{\mu_\ell\}$.

From the last line in Eq. (8), we find that in the thermodynamic limit $N \to \infty$, the free energy is given by

$$f(\mu) = -\lim_{N\to\infty}\frac{1}{N}\ln Z(\mu) = \frac{1}{N}\sum_{l=1}^{N}\ln(\mu-\mu_l). \tag{9}$$

Using the relation $\ln x=\ln|x|+i\pi\theta(-x)$ for x possessing a positive infinitesimal imaginary part, we find that the derivative of the imaginary part of the free energy gives the spectral density function as [30,31]

$$\rho(\mu) = -\frac{2}{\pi}\mathrm{Im}\frac{\partial f}{\partial \mu}. \tag{10}$$

III. RENORMALIZATION-GROUP APPROACH TO GAUSSIAN MODEL

The hierarchical structure of the WF networks allows one to compute the exact partition function of the Gaussian model in Eq. (8) using the RG calculations. When the spin variables of the youngest nodes at the nth generation are integrated out in Eq. (8), the partition function takes the same functional form as that of the previous generation with renormalized parameters. Iterating this decimation procedure and rescaling the variables, we obtain the recursive relations for the parameters, by which we can trace the RG flow. Thus, we obtain the partition function $Z(\mu)$ and the spectral density function of the Laplacian matrix L. Next, we describe the RG calculation of the Gaussian model on the WF networks in detail.

A. Renormalization-group process

Reversing the construction process of the WF networks, we find that the subgraph in Fig. 2, which we call a leaf, reduces to a type-I link. On the other hand, the type-II links outside the leaves remain. All the youngest nodes are inside the leaves, each of which has two old nodes connected by one type-II link and $u+v-2$ youngest nodes connected by type-I links. Therefore, we can make the form of the partition function at the nth generation identical to that at the $(n-1)$th generation by integrating out the spin variables of the youngest nodes in each leaf.

Since the partition function in Eq. (8) can be written as the product of the Boltzmann factors of each link, we find that

$$Z_n(\mu) = \int \mathcal{D}\phi \exp\left[\sum_{(\ell q)} \{-i(1-\mu)(\phi_\ell^2+\phi_q^2) + 2iW_{\ell q}\phi_\ell\phi_q\}\right]. \tag{11}$$

As will be shown, the parameter μ is renormalized differently for the two types of links. So, we introduce distinct

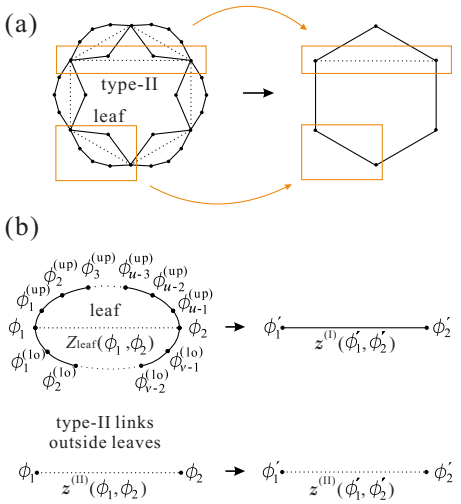

FIG. 2. (Color online) RG of the Gaussian model on the WF networks. (a) Reverse of the construction process for $u=2$ and $v=4$ from $n=2$nd generation to $n=1$st generation. While the type-II link in the upper box remains, each of six *leaves* (one example in the lower box) becomes a type-I link at $n=1$. (b) In one RG step, the spin variables of the $u+v-2$ youngest nodes are integrated out in the partition function $Z_{\rm leaf}$ of each leaf, which is then identical to $z^{(\rm I)}$ with rescaling ϕ's and renormalizing the parameters. The partition function $z^{(\rm II)}$ keeps its form.

parameters μ_1 and μ_2 for different link types such that

$$Z_n(\mu_1,\mu_2,p)=\int \mathcal{D}\phi \prod_{(\ell q)\in E_n^{(\rm I)}} z_n^{(\rm I)}(\phi_\ell,\phi_q) \prod_{(\ell q)\in E_n^{(\rm II)}} z_n^{(\rm II)}(\phi_\ell,\phi_q),$$

where

$$z_n^{(\rm I)}(\phi_\ell,\phi_q)=\exp[-i(1-\mu_1)(\phi_\ell^2+\phi_q^2)+2i\phi_\ell\phi_q],$$

$$z_n^{(\rm II)}(\phi_\ell,\phi_q)=\exp[-i(1-\mu_2)p(\phi_\ell^2+\phi_q^2)+2ip\phi_\ell\phi_q]. \tag{12}$$

It should be noted that $\mu_1=\mu_2=\mu$ initially.

The partition function for a leaf as shown in Fig. 2(b) is defined as

$$\begin{aligned} Z_{\rm leaf}(\phi_1,\phi_2) \equiv z_n^{(\rm II)}(\phi_1,\phi_2)\int \prod_{\ell=1}^{u-1} d\phi_\ell^{(\rm up)} \prod_{q=1}^{v-1} d\phi_q^{(\rm lo)} \\ \times \prod_{\ell=1}^{u-2} z_n^{(\rm I)}(\phi_\ell^{(\rm up)},\phi_{\ell+1}^{(\rm up)}) \prod_{q=1}^{v-2} z_n^{(\rm I)}(\phi_q^{(\rm lo)},\phi_{q+1}^{(\rm lo)}) \\ \times z_n^{(\rm I)}(\phi_1',\phi_1^{(\rm up)}) z_n^{(\rm I)}(\phi_{u-1}^{(\rm up)},\phi_2') z_n^{(\rm I)}(\phi_1',\phi_1^{(\rm lo)}) \\ \times z_n^{(\rm I)}(\phi_{v-1}^{(\rm lo)},\phi_2'). \end{aligned} \tag{13}$$

The number of leaves and the number of remaining type-II links at the nth generation are equal to the numbers of type-I and type-II links of the $(n-1)$th generation, respectively. Thus, the partition function Z_n of the nth generation can be written as

$$Z_n=\int \mathcal{D}\phi \prod_{(\ell q)\in E_{n-1}^{(\rm I)}} Z_{\rm leaf}(\phi_\ell,\phi_q) \prod_{(\ell q)\in E_{n-1}^{(\rm II)}} z_{n-1}^{(\rm II)}(\phi_\ell,\phi_q),$$

which is identical to that of Z_{n-1} if $Z_{\rm leaf}(\phi_1,\phi_2)$ takes the same form as $z_{n-1}^{(\rm I)}(\phi_1,\phi_2)$. It should be noted that there is no change in $z_n^{(\rm II)}(\phi_\ell,\phi_q)$ for $(\ell q)\in E_{n-1}^{(\rm II)}$. The function $Z_{\rm leaf}(\phi_1,\phi_2)$ is evaluated in Appendix B and the result is

$$\begin{aligned} Z_{\rm leaf}(\phi_1,\phi_2)=(\pi i/2)^{(u+v-2)/2}G(\mu_1)^{-1/2} \\ \times\exp[-i\{2(1-\mu_1)+p(1-\mu_2)-h_1(\mu_1)\} \\ \times(\phi_1^2+\phi_2^2)+2i\{p+h_2(\mu_1)\}\phi_1\phi_2], \end{aligned} \tag{14}$$

where

$$c(\ell,a,b)=1-a-\cos(\ell\pi/b),$$

$$G(\mu_1)=\prod_{\ell=1}^{u-1} c(l,\mu_1,u)\prod_{q=1}^{v-1} c(q,\mu_1,v),$$

$$h_1(\mu_1)=\frac{1}{u}\sum_{\ell=1}^{u-1}\frac{\sin^2(\ell\pi/u)}{c(\ell,\mu_1,u)}+\frac{1}{v}\sum_{q=1}^{v-1}\frac{\sin^2(q\pi/v)}{c(q,\mu_1,v)},$$

$$h_2(\mu_1)=\frac{1}{u}\sum_{\ell=1}^{u-1}\frac{(-1)^{\ell-1}\sin^2(\ell\pi/u)}{c(\ell,\mu_1,u)}+\frac{1}{v}\sum_{q=1}^{v-1}\frac{(-1)^{q-1}\sin^2(q\pi/v)}{c(q,\mu_1,v)}. \tag{15}$$

The properties of $G(\mu_1)$, $h_1(\mu_1)$, and $h_2(\mu_1)$ for small μ_1 are given in Appendix C.

Let us introduce the rescaled variables $\phi_\ell'=\phi_\ell/\sqrt{p+h_2(\mu_1)}$. Then, the coefficient of $\phi_1'\phi_2'$ in Eq. (14) becomes 1 and it follows that

$$Z_{\rm leaf}(\phi_1,\phi_2)=(\pi i/2)^{(u+v-2)/2}G(\mu_1)^{-1/2}z_{n-1}^{(\rm I)}(\phi_1',\phi_2'),$$

$$z_n^{(\rm II)}(\phi_1,\phi_2)=z_{n-1}^{(\rm II)}(\phi_1',\phi_2'), \tag{16}$$

with the renormalized parameters μ_1', μ_2', and p'

$$1-\mu_1'=\frac{2(1-\mu_1)+p(1-\mu_2)-h_1(\mu_1)}{p+h_2(\mu_1)},$$

$$\mu_2'=\mu_2,$$

$$p'=\frac{p}{p+h_2(\mu_1)}. \tag{17}$$

The partition function Z_n is then related to Z_{n-1} as

$$Z_n(\mu_1,\mu_2,p)=\exp[-N_n g(\mu_1,p)]Z_{n-1}[\mu_1',\mu_2',p'], \tag{18}$$

where the function $g(\mu_1,p)$ is defined as

$$g(\mu_1,p)=\frac{L_{n-1}^{(\rm I)}}{2N_n}\ln[G(\mu_1)]+\frac{N_{n-1}}{2N_n}\ln[p+h_2(\mu_1)]. \tag{19}$$

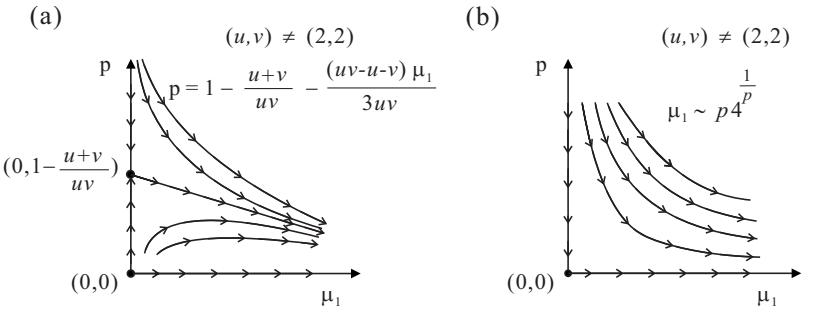

FIG. 3. RG flow in the (μ_1,p) parameter plane. (a) RG flow for $(u,v)\neq(2,2)$. There are two fixed points in the small-μ_1 region: (0,0) and $(0,1-u^{-1}-v^{-1})$. If $p=0$ initially, the flow is outward along the μ_1 axis. When $p\neq 0$ initially, it is first attracted toward $(0,1-u^{-1}-v^{-1})$ and then repelled along the line $p=1-(u+v)/(uv)-\mu_1(uv-u-v)/(3uv)$. (b) RG flow for $(u,v)=(2,2)$. There is a fixed point at the origin and the flow follows a curve $\mu_1\sim p4^{1/p}$.

As this RG transformation is repeated, the parameters μ_1 and p are renormalized successively according to Eq. (17). The parameter μ_2 remains at its initial value μ. On the other hand, the parameter μ_1 is renormalized in a nontrivial way.

B. Fixed points and RG flow

Here, we investigate the RG flow in the small-μ_1 region in the (μ_1,p) parameter space from the recursive relations (17). The RG flow will help to understand the change by shortcuts. For example, if there is only one fixed point at $p=0$, then the spectral dimension d_s would be the same regardless of the shortcut weight p. Otherwise, d_s can be changed from the one with $p=0$.

For small μ_1, one finds two fixed points in the (μ_1,p) plane located at

$$(\mu_1^*,p^*)=(0,0),\ \ (0,1-u^{-1}-v^{-1}). \tag{20}$$

These two fixed points meet when $(u,v)=(2,2)$. Let us first consider the case $(u,v)\neq(2,2)$. Near the fixed point $(\mu_1^*=0,\ \ p^*=0)$, the RG equation (17) is linearized as

$$\mu_1'=uv\mu_1,\quad p'=\frac{uv}{u+v}p, \tag{21}$$

and therefore, after τ RG transformations, μ_1 and p take the following values:

$$\mu_1^{(\tau)}=(uv)^\tau\mu,\quad p^{(\tau)}=\left(\frac{uv}{u+v}\right)^\tau p. \tag{22}$$

Since uv and $uv/(u+v)$ are not smaller than 1 for $u\geq 2$ and $v\geq 2$, the fixed point (0,0) is unstable. Around the other fixed point $(\mu_1^*=0,\ \ p^*=1-u^{-1}-v^{-1})$, the linearized RG equation is written as

$$\begin{pmatrix}\mu_1'\\ p'-p^*\end{pmatrix}=R\begin{pmatrix}\mu_1\\ p-p^*\end{pmatrix}+\mu\begin{pmatrix}1-u^{-1}-v^{-1}\\ 0\end{pmatrix},$$

where

$$R=\begin{pmatrix}u+v & 0\\ -\dfrac{(uv-u-v)(uv-1)(u+v)}{3(uv)^2} & \dfrac{u+v}{uv}\end{pmatrix}. \tag{23}$$

The matrix R has two eigenvalues $u+v$ and $(u+v)/(uv)$ and the parameters after τ RG transformations are given by

$$\mu_1^{(\tau)}=\mu\left[\frac{(u+v)(uv-1)}{uv(u+v-1)}\{(u+v)^\tau-1\}+1\right],$$

$$p^{(\tau)}-p^*=\mu\frac{(u+v)(uv-1)(uv-u-v)}{3(uv)^2(u+v-1)}\{1-(u+v)^\tau\}+(p-p^*)\left(\frac{u+v}{uv}\right)^\tau. \tag{24}$$

If $(u,v)=(2,2)$, there is only one fixed point at $(\mu_1^*=0,\ \ p^*=0)$ for small μ_1. The renormalized value $p^{(\tau)}$ can be calculated from Eq. (17) as

$$p^{(\tau)}=\frac{1}{\tau+p^{-1}}. \tag{25}$$

It should be noted that $p^{(\tau)}$ is not as small as μ. Inserting Eq. (25) into Eq. (17), a recursive relation for μ_1 is obtained, which can be solved to give

$$\mu_1^{(\tau)}=\frac{(1+3p^{-1})4^\tau-1}{3(\tau+p^{-1})}\mu. \tag{26}$$

To understand the renormalization of μ_1 and p, which depends on their initial values as well as the network model parameters u and v, we consider the following three cases:

$$\text{(I)}\quad p=0,$$

$$\text{(II)}\quad p\neq 0,\quad (u,v)\neq(2,2),$$

$$\text{(III)}\quad p\neq 0,\quad (u,v)=(2,2).$$

(I) If $p=0$ initially, p remains at zero and μ_1 increases according to Eq. (22). (II) If $p>0$ initially and $(u,v)\neq(2,2)$, both μ_1 and p increase by Eq. (22) and the RG flow runs outward from (0,0) along the curve $p\sim\mu_1^{1-\ln(u+v)/\ln(uv)}$ as obtained from Eq. (22). The RG flow then runs toward the other fixed point $(0,1-u^{-1}-v^{-1})$, driven by one eigenvalue $(u+v)/(uv)<1$ of R in Eq. (23). Once p gets sufficiently close to p^*, the RG flow is bent outward along the line $p-p^*=-\mu_1[uv-(u+v)]/(3uv)$, parallel to the other eigenvector of R [see Fig. 3(a)]. (III) When $(u,v)=(2,2)$, the two fixed points coincide each other. The RG flow along the p

axis runs quite slowly as the corresponding eigenvalue of R is 1. If $p=0$, μ_1 and p are renormalized in the same way as in case (I). If $p\neq 0$, the RG flow runs along the curve $\mu_1 \sim p4^{1/p}$ as obtained from Eq. (26), which is depicted in Fig. 3(b).

C. Spectral density function and spectral dimension

The free energy per node in the thermodynamic limit $f(\mu)=-\lim_{n\to\infty} N_n^{-1} \ln Z_n(\mu,\mu,p)$ can be obtained by using $g(\mu_1,p)$ in Eq. (19) as [32]

$$f(\mu)=\sum_{\tau=0}^{\infty}\frac{g(\mu_1^{(\tau)},p^{(\tau)})}{(u+v)^{\tau}}, \tag{27}$$

where we used $N_{n-1}/N_n \simeq (u+v)^{-1}$ for large n. Using the expansion of the functions $G(\mu_1)$ and $h_2(\mu_1)$ given in Appendix B, we can obtain the expansion of $g(\mu_1^{(\tau)},p^{(\tau)})$ up to the first order in $\mu_1^{(\tau)}$ and $p^{(\tau)}-p^*$ as

$$g(\mu_1^{(\tau)},p^{(\tau)}) \simeq \frac{1}{2(u+v)(u+v-2)}\left[\ln[G(0)]+\ln\left(1-\frac{\mu_1^{(\tau)}}{\mu_{c1}}\right)\right]+\frac{1}{2(u+v)}\left[\ln[G(0)\{p^*+u^{-1}+v^{-1}\}]+\ln\left(1+\frac{p^{(\tau)}-p^*+\mu_1^{(\tau)}\dfrac{(uv-1)(u+v)}{3uv}}{p^*+u^{-1}+v^{-1}}-\frac{\mu_1^{(\tau)}}{\mu_{c1}}\right)\right], \tag{28}$$

where we used $L_{n-1}/N_n \simeq (u+v-1)/[(u+v)(u+v-2)]$ and introduced a constant

$$\mu_{c1}=\frac{3}{u^2+v^2-2}. \tag{29}$$

The renormalized values of μ_1 and p obtained above for each of cases (I)–(III) can be used in Eqs. (27) and (28) to evaluate the free energy $f(\mu)$.

For case (I), the shortcuts have no weight and the network is a fractal as long as $u\geq 2$ and $v\geq 2$. The parameter p remains at zero under the RG transformation and μ_1 is renormalized by Eq. (22). Inserting Eq. (22) in Eqs. (27) and (28) with $p^{(\tau)}=p^*=0$, we obtain the free energy and then the spectral density function via Eq. (10), which is calculated as

$$\begin{aligned}\rho_{(\mathrm{I})}(\mu) &\simeq \frac{2}{\pi}\mathrm{Im}\sum_{\tau=0}^{\infty}\frac{\partial\mu_1^{(\tau)}}{\partial\mu}\frac{\dfrac{\partial}{\partial\mu_1^{(\tau)}}g(\mu_1^{(\tau)},0)}{(u+v)^{\tau}}\\ &\simeq \int_1^{\infty}dz\frac{\dfrac{\delta(z-\mu_{c1}/\mu)}{(u+v)(u+v-2)}+\dfrac{\delta(z-\mu_{c2}/\mu)}{u+v}}{\mu\ln(uv)z^{\ln(u+v)/\ln(uv)}}\\ &\simeq \kappa_{(\mathrm{I})}\mu^{\{[\ln(u+v)]/[\ln(uv)]\}-1},\end{aligned} \tag{30}$$

where

$$\mu_{c2}=\frac{3}{u^2+v^2-uv-1},$$

$$\kappa_{(\mathrm{I})}=\frac{((u+v-2)^{-1}\mu_{c1}^{-\ln(u+v)/\ln(uv)}+\mu_{c2}^{-\ln(u+v)/\ln(uv)})}{(u+v)\ln(uv)}.$$

Comparing Eq. (5) with Eq. (30), we find that the spectral dimension d_s for case (I) is

$$d_s^{(\mathrm{I})}=\frac{2\ln(u+v)}{\ln(uv)}. \tag{31}$$

This is consistent with the previous result obtained for the mean first passage time studied in Ref. [23]. The spectral dimension in Eq. (31) is reduced to 2 when $u=v=2$ and ranges between 1 and 2 when u and v differ from 2. It should be noted that it is different from the fractal dimension given in Eq. (2).

For case (II), the RG flow starting from a point with nonzero values of μ_1 and p first approaches the fixed point $(0,1-u^{-1}-v^{-1})$, and then it is repelled in the direction of one eigenvector of the matrix R in Eq. (23) as shown in Fig. 3(a). Using Eq. (24) and setting $p^*=1-u^{-1}-v^{-1}$ in Eqs. (27) and (28), we obtain the spectral density function

$$\begin{aligned}\rho_{(\mathrm{II})}(\mu) &\simeq \frac{2}{\pi}\mathrm{Im}\sum_{\tau=0}^{\infty}\frac{\partial}{\partial\mu}\frac{\dfrac{\partial}{\partial\mu_1^{(\tau)}}g(\mu_1^{(\tau)},p^{(\tau)})}{(u+v)^{\tau}}\\ &\simeq \int_1^{\infty}dz\frac{\dfrac{\delta\left(z-\dfrac{\mu_{c1}}{\mu c}\right)}{(u+v)(u+v-2)}+\dfrac{\delta\left(z-\dfrac{\mu_{c3}}{\mu}\right)}{(u+v)}}{z\mu\ln(u+v)}\simeq\kappa_{(\mathrm{II})},\end{aligned} \tag{32}$$

where

$$c = \frac{(u+v)(uv-1)}{(uv)(u+v-1)},$$

$$\mu_{c3} = \frac{3uv(u+v-1)}{(uv-1)(u+v)(u^2+v^2-u-v-1)},$$

$$\kappa_{(\mathrm{II})} = \frac{(uv-1)(u^2+v^2-u-v)}{3uv(u+v-2)\ln(u+v)}.$$

It should be noted that $\rho_{(\mathrm{II})}(\mu)$ is independent of p since the p-dependent term in Eq. (24) is vanishing in the $\tau\to\infty$ limit. For case (II), $\rho(\mu)$ is a constant for small μ, which indicates that

$$d_s^{(\mathrm{II})} = 2. \tag{33}$$

This means that the spectral dimension is changed by the addition of shortcuts. Remarkably d_s remains at 2 regardless of u or v.

For case (III), there is only one fixed point and $p^{(\tau)}$ remains to be $\mathcal{O}(1)$. Inserting Eqs. (25) and (26) in Eqs. (27) and (28) with $p^*=0$, the spectral density function for $u=v=2$ is calculated as

$$\begin{aligned}\rho_{(\mathrm{III})}(\mu) &\simeq \frac{2}{\pi}\mathrm{Im}\sum_{\tau=0}^{\infty}\frac{\partial\mu_1^{(\tau)}}{\partial\mu}\frac{\frac{\partial}{\partial\mu_1^{(\tau)}}g(\mu_1^{(\tau)},p^{(\tau)})}{(u+v)^{\tau}}\\ &\simeq \int_1^{\infty}\frac{dz}{\mu z\ln 4}\left[\frac{1}{8}\delta\left(z-\frac{\mu_{c1}}{\mu}\frac{3(1+p\log_4 z)}{p+3}\right)\right.\\ &\quad\left.+\frac{1}{4}\delta\left(z-\frac{1}{\mu}\frac{3(1+p\log_4 z)}{p+3}\right)\right]\\ &\simeq \frac{p+3}{6\ln 4}\frac{1}{1+p\log_4(1/\mu)}.\end{aligned} \tag{34}$$

We remark that Eq. (34) with $p=0$ is reduced to Eq. (30). On the other hand, for $p>0$, the spectral density function takes a logarithmic form, $\rho(\mu)\sim[\ln(1/\mu)]^{-1}$ for $\mu\to 0$. In the scaling regime where $\mu\exp(p^{-1})$ is finite, the spectral density function displays the following crossover behavior:

$$\rho_{(\mathrm{III})}(\mu) \simeq \begin{cases}\dfrac{p+3}{6p}\dfrac{1}{\log_4(1/\mu)} & \text{for } \mu e^{p^{-1}} \ll 1\\ \dfrac{p+3}{6\ln 4} & \text{for } \mu e^{p^{-1}} \gg 1.\end{cases} \tag{35}$$

IV. RETURN-TO-ORIGIN PROBABILITY

In this section, we derive the RTO probability $P_o(t)$ of the RWs from the spectral density function $\rho(\mu)$ obtained in the previous section. The behavior of $\rho(\mu)$ around $\mu=2$, which should be known for Eq. (4), can be understood by the symmetry property of the RG equation (17). First, let us consider two cases: (i) When both u and v are odd, $G(\mu_1)$ and $h_2(\mu_1)$ are symmetric and $h_1(\mu_1)$ is antisymmetric with respect to $\mu_1=1$. Thus, the variables $\tilde{\mu}_1\equiv 2-\mu_1$ and p are renormalized in the same manner as in Eqs. (22) and (24) around the fixed points $(\tilde{\mu}_1^*=2,\ p^*=0)$ and $(\tilde{\mu}_1^*=2,\ p^*=1-u^{-1}-v^{-1})$, respectively. This leads to $\rho(2-\mu)=\rho(\mu)$. (ii) When $p=0$ and both u and v are even, $G(\mu_1)$ is symmetric and $h_1(\mu_1)$ and $h_2(\mu_1)$ are antisymmetric with respect to μ_1. Interestingly, the parameter μ_1, initially close to 2, is renormalized by one RG transformation to a value near zero by Eq. (17) and then follows the same RG flow as given in Eqs. (22) and (24). Therefore, the spectral density function is symmetric about $\mu=1$. In these two cases (i) and (ii), it follows that

$$P_o(t) \simeq (1+(-1)^t)\int_0^{\infty} d\mu\rho(\mu)e^{-\mu t}. \tag{36}$$

For cases other than case (i) or (ii), there is no fixed point on the line $\mu_1=2$; thus, the contribution of $\rho(\mu)$ around $\mu=2$ to $P_o(t)$ for large t is subdominant, leading to

$$P_o(t) \simeq \int_0^{\infty} d\mu\rho(\mu)e^{-\mu t}. \tag{37}$$

Taking into account different behaviors of $\rho(\mu)$ for small μ in cases (I)–(III), we obtain the following from Eq. (4):

$$P_o(t) \simeq p_o\begin{cases}\kappa_{(\mathrm{I})}\Gamma(d_s^{(\mathrm{I})}/2)t^{-d_s^{(\mathrm{I})}/2} & (\mathrm{I})\\ \kappa_{(\mathrm{II})}t^{-1} & (\mathrm{II})\\ \dfrac{p+3}{6\ln 4}t^{-1}(1+p\log_4 t)^{-1} & (\mathrm{III}),\end{cases} \tag{38}$$

where $\Gamma(x)$ is the gamma function and the spectral dimension $d_s^{(\mathrm{I})}$ in case (I) is given in Eq. (31). It should be noted that for case (III), a logarithmic term appears. As discussed above, the coefficient p_o is 2 when both u and v are odd or when $p=0$ and both u and v are even. Otherwise, it is 1.

In order to check Eq. (38), we performed numerical simulations of RWs on the WF networks with various values of u, v, and p. In the simulations, WF networks that were grown up to $n=(5-7)$th generation were used, which contained 10^4-10^5 nodes, depending on the values of u and v, as listed in Table I. For each of the WF networks, we put $M=10^6$ random walkers at randomly chosen nodes and allowed them to move around independently (without interacting with each other). Thus, we could record the positions $\ell_t^{(r)}$ of 10^6 random walkers at time t, where r is the index of the random walker. A RWer at node q at time t moves to a randomly selected neighboring node q' with probability $W_{q'q}/s_q$, in which $W_{q'q}$ is the link weight, and $s_q=\Sigma_{q'}W_{q'q}$ is the node strength. All RWers are updated in this manner. Then, the RTO probability $P_o(t)$ can be obtained by counting the number of RWers found at their respective initial positions $\ell_0^{(r)}$ at time t:

$$P_o(t) = \frac{1}{M}\sum_{r=1}^{M}\delta_{\ell_t^{(r)},\ell_0^{(r)}}. \tag{39}$$

The measured RTO probabilities for various values of p and (u,v) are shown in Fig. 4. The spectral dimension is obtained from the power-law decay of $P_o(t)$. When the shortcuts have zero weight, i.e., $p=0$, the measured values of d_s for various u's and v's are in good agreement with Eq. (31)

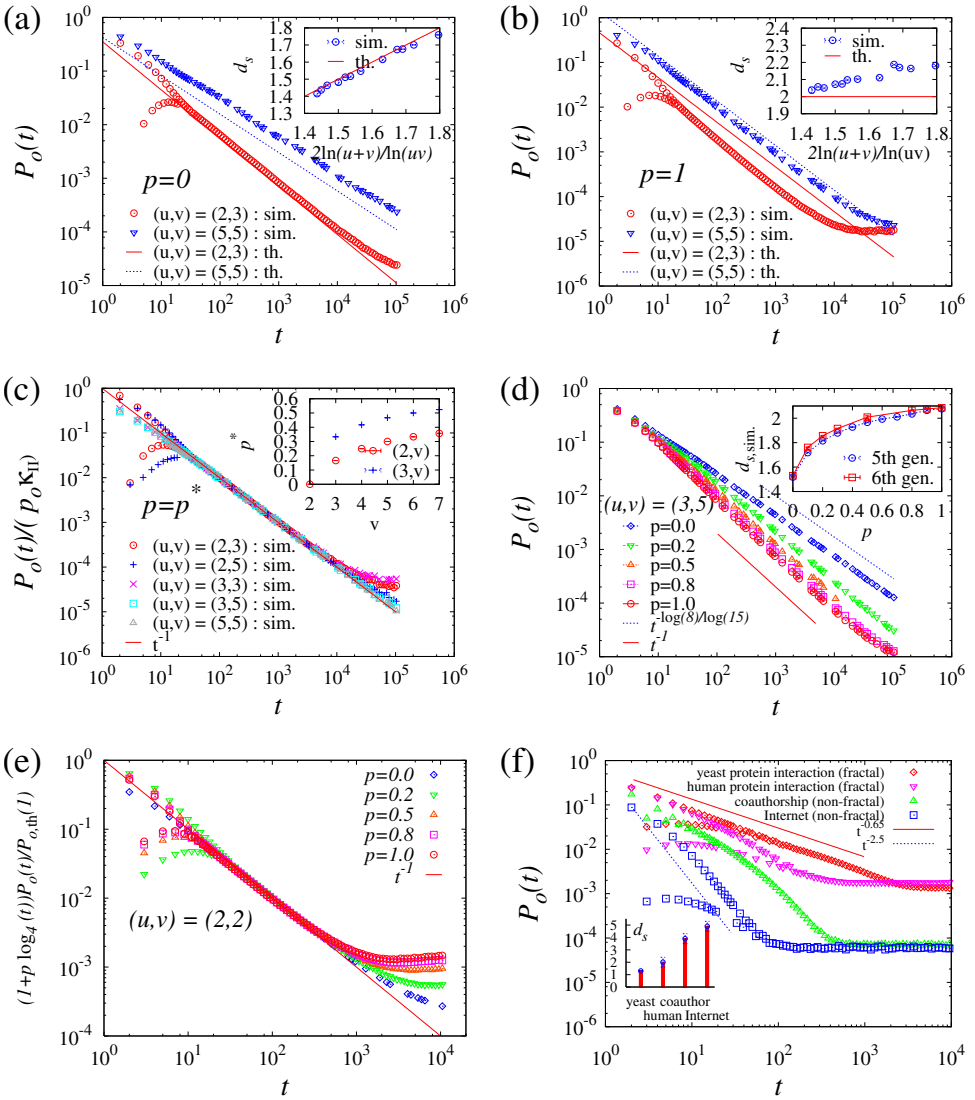

FIG. 4. (Color online) Return-to-origin probability $P_o(t)$ on WF networks. (a) Plots of $P_o(t)$ on the fractal WF networks ($p=0$). Simulation results for $(u,v)=(2,3)$ and $(u,v)=(5,5)$ are shown and the lines represent the theoretical prediction in Eq. (38). (Inset) Plot of the spectral dimension d_s as a function of $2\ln(u+v)/\ln(uv)$. The values of d_s were estimated from $P_o(t)$ for $(u,v)=(2,3)$, (2,4), (2,6), (3,3), (3,4), (3,5), (3,6), (4,4), (4,5), (4,6), and (5,5) using the relation $P_o(t)\sim t^{-d_s/2}$. The line represents the analytical prediction $d_s=2\ln(u+v)/\ln(uv)$. (b) Plots of $P_o(t)$ on the nonfractal WF networks ($p=1$) for the same values of u and v. The lines represent the theoretical predictions in Eq. (38). (Inset) Plot of the spectral dimension d_s as a function of $2\ln(u+v)/\ln(uv)$. The line represents the analytical prediction $d_s=2$. (c) Plots of $P_o(t)/(p_o\kappa_{II})$ on the nonfractal WF networks for $p=p^*$ and various values of u and v. All the data points collapse to t^{-1} as predicted by Eq. (38). (Inset) Plot of the fixed point p^* as a function of v for u fixed at 2 and 3. This shows that as v increases, p^* approaches 1. (d) Plots of $P_o(t)$ for $(u,v)=(3,5)$ and various values of p. The slopes of the two lines are $-\ln 8/\ln 15$ and -1, corresponding to the analytical prediction for $d_s/2$ for $p=0$ and $p=1$ for $(u,v)=(3,5)$. (Inset) Plot of the spectral dimension d_s as a function of p. The results obtained for the fifth and sixth generations are presented. (e) Plots of $(1+p\log_4 t)P_o(t)/P_{o,\mathrm{th}}(1)$ versus t for $(u,v)=(2,2)$ and $p=0$, 0.2, 0.5, 0.8, and 1, where $P_{o,\mathrm{th}}(1)=p_o(p+3)/(6\ln 4)$. All the data points collapse to t^{-1} as predicted by Eq. (38). (f) Plots of $P_o(t)$ on real-world networks. The two lines are the guide for the eye, and the spectral dimensions read from the slope of the log-log plots of $P_o(t)$ are given in the inset.

[see Fig. 4(a)]. Our results for the spectral dimension of the fractal WF networks ($p=0$) confirm the previous results obtained in the study of the mean first passage time [23].

When $p=1$, the numerical values of d_s are somewhat larger than the theoretical value of 2, in the range of 2–2.2, and the coefficient $(p_0\kappa_{(\mathrm{II})})$ in Eq. (38) seems to deviate from the numerical result, especially for $(u,v)=(2,3)$, as seen in Fig. 4(b). These differences come from the finite-size effect. As the RG transformation is repeated, the parameter p is renormalized, as seen in Eq. (24) or Fig. 3(a). When μ is sufficiently small, which is the case here, p approaches the fixed point p^* and is then repelled. The RG transformation is based on the assumption that $p-p^*$ is sufficiently small; thus, we can derive the recursive relations of the parameters in a series of $p-p^*$. However, when the system size is finite, only a finite number of RG transformations can be made and

$p-p^*$ cannot be sufficiently small. In this case, the iterations of recursive relations with a linear term of $p-p^*$ may not be justified. This truncation causes the discrepancy that we observed. When u and v are larger, such that p^* is close to $p=1$, or when we start from a smaller value of p for a given (u,v), $p-p^*$ can be smaller even for finite RG steps, and then the discrepancy reduces, as observed in Figs. 4(b) and 4(c), respectively. In Fig. 4(c), we plot $P_o(t)/(p_o\kappa_{(\mathrm{II})})$ as a function of t for $p=p^*$ and various values of (u,v); all the data points collapse perfectly onto t^{-1} as predicted by Eq. (38).

The case of $0<p<1$ is also interesting. For $(u,v)\neq(2,2)$, d_s increases rapidly with p, as shown for $(u,v)=(3,5)$ in Fig. 4(d). It should be noted that d_s is 2 when $p=p^*=1-\frac{1}{u}-\frac{1}{v}\sim 0.47$ for $u=3$ and $v=5$. As p deviates from the fixed-point value, the finite-size effect is expected to make d_s deviate slightly from 2. In the inset of Fig. 4(d), it is shown that the plot of d_s versus p looks more concave as N increases.

For $(u,v)=(2,2)$, the RTO probability is expected to have a logarithmic term, $P_o(t)\simeq P_{o,\mathrm{th}}(1)t^{-1}(1+p\,\log_4 t)^{-1}$ with $P_{o,\mathrm{th}}(1)=p_o(p+3)/(6\ln 4)$. We plot $(1+p\,\log_4 t)P_o(t)/P_{o,\mathrm{th}}(1)$ versus t for various values of p in Fig. 4(d), in which the data are well collapsed onto t^{-1} as predicted in Eq. (38).

The RTO probability and the spectral dimension of the nonfractal WF networks with $p\neq 0$ were obtained in this work. We were able to identify the effect of shortcuts on the random-walk dynamics. The faster decay of $P_o(t)$ and the larger spectral dimension for $p\neq 0$ than for $p=0$ are caused by shortcuts. Remarkably, when the shortcuts have nonzero weight, other structural factors such as the degree distribution do not affect the spectral dimension, in contrast with the fractal case $p=0$.

We also performed numerical simulations of RWs on the following real-world complex networks: the protein interactions network of yeast [33], the human protein interaction network [34], the coauthorship network of the cond-mat archive [35], and the Internet at the autonomous system level [36]. While these networks have different structures from the WF networks, their spectral dimensions, presented in Fig. 4(f), were much larger for nonfractal networks than for fractal networks, as identified for the WF networks. The two protein interaction networks are known as fractals and both the coauthorship network and the Internet are nonfractals [37]. The numerical values of d_s were approximately 1.30 ± 0.04 and 2.0 ± 0.4 for the yeast and the human protein interaction network, respectively, and 3.9 ± 0.4 and 4.9 ± 0.4 for the coauthorship network and the Internet, respectively.

V. SUMMARY AND DISCUSSION

In this paper, we have obtained the exact solution for the RTO probability of RWs and the spectral density function of the Laplacian matrix in hierarchical scale-free networks by applying the RG approach to a Gaussian model. Particularly, we monitored the spectral dimension as we controlled the weight of the shortcuts. When the shortcut weight is zero, the network is a fractal, and its spectral dimension varies in the range (1,2]. This depends on the parameters controlling the network structure. On the other hand, when the weight is larger than zero, the spectral dimension is 2, which is robust under structural variations. This result demonstrates that shortcuts strongly affect the RW motion even when the shortcut weight is small.

It was shown that the organization of shortcuts in a network is essential in the classification of network structures [19]. Let $p(r)$ denote the probability of finding a shortcut between a pair of nodes separated by a distance r. If the decay of $p(r)$ is slower than r^{-2d_f} with d_f being the fractal dimension of the network, the network is renormalized to the complete graph. Otherwise, the network is renormalized to the corresponding fractal network. For the nonfractal WF networks, our results show that $p(r)\sim r^{-\alpha}$, where α/d_f is between 1.6 and 2. Thus, the hierarchical networks with shortcuts belong to the former case, which can be related to our finding that the spectral dimension d_s is robust against the variation in u or v in the $p>0$ regime.

The probability R that a RWer will ever return to the origin is related to the RTO probability as $R=1-1/\Sigma_{t=0}^{\infty}P_o(t)$; thus, RWs are recurrent (transient) if $d_s\leq 2$ ($d_s\geq 2$) [1–3]. In this sense, the structure of the hierarchical networks with shortcuts studied in this work, having $d_s=2$, is marginal in the RW motion; RWers can never return to the origin if the network structure is more interconnected. It would be interesting to observe the results in the case of the Internet. Because the spectral dimension is larger than 2 for the Internet, packets roaming on the Internet may not return to their origin or to a specific destination if they follow the RW motion. Therefore, the studied hierarchical network could be a good sample for the construction of the Internet.

ACKNOWLEDGMENTS

This work was supported by NRF research grants funded by the MEST [Grants No. 2010-0015066 (B.K.) and No. 2010-0015197 (D.-S.L.)] and by the NAP of KRCF (D.-S.L. and D.K.). D.-S.L. acknowledges the TJ Park Foundation for support.

APPENDIX A: OTHER LAPLACIANS

The Laplacian matrix L, defined as $L_{\ell q}=\delta_{\ell q}-W_{\ell q}/s_q$, can be brought into a symmetric form by a similarity transformation $\tilde{L}=SLS^{-1}$, where $S_{\ell q}=s_q^{-1/2}\delta_{\ell q}$ [30],

$$\tilde{L}_{\ell q}=\delta_{\ell q}-\frac{1}{\sqrt{s_\ell s_q}}W_{\ell q}. \tag{A1}$$

The eigenvalues of $\tilde{L}$ and L are identical. Another Laplacian matrix $L'_{\ell q}=s_\ell\delta_{\ell q}-W_{\ell q}$ [30] has different eigenvalues from L or $\tilde{L}$. We consider $\tilde{L}$ in Eq. (A1) for our analysis of the RW problem but the main results also hold for $\tilde{L}$ [38].

APPENDIX B: DERIVATION OF Eq. (14)

In this appendix, we derive the partition function $Z_{\mathrm{leaf}}(\phi'_1,\phi'_2)$ in Eq. (14) for a leaf in Fig. 1(b). Using Eq. (12), we can represent $Z_{\mathrm{leaf}}(\phi'_1,\phi'_2)$ as

$$
\begin{aligned}
&Z_{\mathrm{leaf}}(\phi_1',\phi_2') \\
&= z_n^{(\mathrm{II})}(\phi_1',\phi_2')\int \prod_{\ell=1}^{u-1} d\phi_\ell^{(\mathrm{up})} \prod_{q=1}^{v-1} d\phi_q^{(\mathrm{lo})} \prod_{\ell=1}^{u-2} z_n^{(\mathrm{I})}(\phi_\ell^{(\mathrm{up})},\phi_{\ell+1}^{(\mathrm{up})}) \prod_{q=1}^{v-2} z_n^{(\mathrm{I})}(\phi_q^{(\mathrm{lo})},\phi_{q+1}^{(\mathrm{lo})}) z_n^{(\mathrm{I})}(\phi_1',\phi_1^{(\mathrm{up})}) z_n^{(\mathrm{I})}(\phi_{u-1}^{(\mathrm{up})},\phi_2') z_n^{(\mathrm{I})}(\phi_1',\phi_1^{(\mathrm{lo})}) z_n^{(\mathrm{I})}(\phi_{v-1}^{(\mathrm{lo})},\phi_2') \\
&= z_n^{(\mathrm{II})}(\phi_1',\phi_2')\int \prod_{\ell=1}^{u-1} d\phi_\ell^{(\mathrm{up})} \prod_{q=1}^{v-1} d\phi_q^{(\mathrm{lo})} \\
&\quad \times \exp\left[-i\sum_{\ell,q=1}^{u-1} \phi_\ell^{(\mathrm{up})} \bar{H}_{\ell q}^{(\mathrm{up})} \phi_q^{(\mathrm{up})} - i\sum_{\ell,q=1}^{v-1} \phi_\ell^{(\mathrm{lo})} \bar{H}_{\ell q}^{(\mathrm{lo})} \phi_q^{(\mathrm{lo})} + 2i\phi_1'(\phi_1^{(\mathrm{up})}+\phi_1^{(\mathrm{lo})}) + 2i\phi_2'(\phi_{u-1}^{(\mathrm{up})}+\phi_{v-1}^{(\mathrm{lo})}) - 2i(1-\mu_1)(\phi_1'^2+\phi_2'^2) \right].
\end{aligned}
\tag{B1}
$$

Here, we introduced a $(u-1)\times(u-1)$ Hamiltonian $\bar{H}^{(\mathrm{up})}$ and a $(v-1)\times(v-1)$ Hamiltonian $\bar{H}^{(\mathrm{lo})}$, both of which take a form

$$
\bar{H} = \begin{pmatrix}
H_0 & -1 & 0 & \cdots & \cdots & \cdots & 0 \\
-1 & H_0 & -1 & 0 & \cdots & \cdots & 0 \\
0 & -1 & H_0 & -1 & 0 & \cdots & 0 \\
\cdots & & \cdots & & \cdots & & \cdots \\
0 & \cdots & \cdots & \cdots & 0 & -1 & H_0
\end{pmatrix}, \tag{B2}
$$

with $H_0=2(1-\mu_1)$. The $(n-1)\times(n-1)$ matrices in this form have $n-1$ eigenvalues λ_ℓ and the corresponding eigenvectors $\mathbf{e}_\ell$ with $\ell=1,2,\ldots,n-1$ [39],

$$
\lambda_\ell = H_0 - 2\cos\left(\frac{\ell\pi}{n}\right),
$$

$$
\mathbf{e}_\ell = \sqrt{\frac{2}{n}}\left[\sin\left(\frac{\ell\pi}{n}\right),\sin\left(\frac{2\ell\pi}{n}\right),\ldots,\sin\left(\frac{(n-1)\ell\pi}{n}\right)\right]. \tag{B3}
$$

Therefore, $\bar{H}^{(\mathrm{up})}$ and $\bar{H}^{(\mathrm{lo})}$ are diagonalized with the bases

$$
\tilde{\phi}_\ell^{(\mathrm{up})} = \sqrt{\frac{2}{u}}\sum_{q=1}^{u-1} \sin\left(\frac{\ell q\pi}{u}\right)\phi_q^{(\mathrm{up})},
$$

$$
\tilde{\phi}_\ell^{(\mathrm{lo})} = \sqrt{\frac{2}{v}}\sum_{q=1}^{v-1} \sin\left(\frac{\ell q\pi}{v}\right)\phi_q^{(\mathrm{lo})}, \tag{B4}
$$

respectively, and $Z_{\mathrm{leaf}}(\phi_1',\phi_2')$ is rewritten as

$$
\begin{aligned}
Z_{\mathrm{leaf}}(\phi_1',\phi_2') &= \exp[-i(1-\mu_2)p(\phi_1'^2+\phi_2'^2)+2ip\phi_1'\phi_2'] \int \prod_{\ell=1}^{u-1} d\tilde{\phi}_\ell^{(\mathrm{up})} \prod_{q=1}^{v-1} d\tilde{\phi}_q^{(\mathrm{lo})} \exp\left[-i\sum_{\ell=1}^{u-1} \lambda_\ell (\tilde{\phi}_\ell^{(\mathrm{up})})^2 - i\sum_{q=1}^{v-1} \lambda_q (\tilde{\phi}_q^{(\mathrm{lo})})^2 \right. \\
&\quad \left. + 2i(\phi_1'+\phi_2')\left\{ \sqrt{\frac{2}{u}}\sum_{\ell=1}^{u-1} \sin\left(\frac{\ell\pi}{u}\right)\tilde{\phi}_\ell^{(\mathrm{up})} + \sqrt{\frac{2}{v}}\sum_{q=1}^{v-1} \sin\left(\frac{q\pi}{v}\right)\tilde{\phi}_q^{(\mathrm{lo})} \right\} - 2i(1-\mu_1)(\phi_1'^2+\phi_2'^2) \right],
\end{aligned}
\tag{B5}
$$

which is calculated to give Eq. (14). It should be noted that $c(\ell,a,b)$ in Eq. (15) is half the eigenvalue λ_ℓ in Eq. (B3) with $n=b$ and $H_0=2(1-a)$.

APPENDIX C: EXPANSION OF $G(\mu_1)$, $h_1(\mu_1)$, AND $h_2(\mu_1)$ IN EQ. (15)

The small-μ_1 behaviors of $G(\mu_1)$, $h_1(\mu_1)$, and $h_2(\mu_1)$ are used to linearize Eq. (17) and to find the small-μ_1 behaviors of $g(\mu_1,p)$ in Eq. (19). Expanding these functions for small μ_1 up to the first order, we obtain

$$
G(\mu_1) = G(0)\left[1 - \frac{\mu_1}{2}\{S_1(u)+S_1(v)\}\right] + \mathcal{O}(\mu_1^2), \tag{C1}
$$

$$
\begin{aligned}
h_1(\mu_1) &= \frac{u-1}{u} + \frac{v-1}{v} \\
&\quad + \mu_1\left[\frac{S_1(u)-(u-1)}{u} + \frac{S_1(v)-(v-1)}{v}\right] + \mathcal{O}(\mu_1^2),
\end{aligned}
$$

$$h_2(\mu_1) = \frac{1}{u} + \frac{1}{v} + \mu_1 \left[\frac{S_2(u) - \frac{1+(-1)^u}{2}}{u} + \frac{S_2(v) - \frac{1+(-1)^v}{2}}{v} \right] + \mathcal{O}(\mu_1^2), \tag{C2}$$

where $G(0) = \Pi_{\ell=1}^{u-1}[1-\cos(\ell\pi/u)]\Pi_{q=1}^{v-1}[1-\cos(q\pi/v)]$ and we introduced two sums $S_1(n)$ and $S_2(n)$ defined as

$$S_1(n) = \sum_{j=1}^{n-1} \frac{1}{\sin^2\left(\frac{j\pi}{2n}\right)},$$

$$S_2(n) = \sum_{j=1}^{n-1} \frac{(-1)^{j+1}}{\sin^2\left(\frac{j\pi}{2n}\right)}. \tag{C3}$$

To compute $S_1(n)$ and $S_2(n)$, we use the following identity:

$$\frac{1}{\sin^2(\pi a)} = \frac{1}{\pi^2} \sum_{k=-\infty}^{\infty} \frac{1}{(k-a)^2}, \tag{C4}$$

which can be derived by considering the following integral on a circle with radius R of which goes to infinity:

$$\int dz \frac{\cot(\pi z)}{(z-a)^2} = i\left\{ \sum_{n=-\infty}^{\infty} \frac{1}{(n-a)^2} - \frac{\pi^2}{\sin^2(\pi a)} \right\} = 0. \tag{C5}$$

Using Eq. (C4), the sum $S_1(n)$ is evaluated as

$$S_1(n) = \sum_{j=1}^{n-1} \frac{1}{\sin^2\left(\frac{j\pi}{2n}\right)} = \frac{1}{2}\sum_{j=1}^{n-1}\left(\frac{1}{\sin^2\left(\frac{j\pi}{2n}\right)} + \frac{1}{\sin^2\left(\pi - \frac{j\pi}{2n}\right)} \right)$$
$$= \frac{1}{2\pi^2}\sum_{j=1}^{n-1}\sum_{k=-\infty}^{\infty}\left(\frac{1}{\left(\frac{j}{2n}-k\right)^2} + \frac{1}{\left(1-\frac{j}{2n}-k\right)^2} \right)$$
$$= \frac{4n^2}{\pi^2}\sum_{s=1}^{\infty}\left(\frac{1}{s^2} - \frac{1}{(sn)^2} \right) = \frac{2(n^2-1)}{3}. \tag{C6}$$

Similarly, the sum $S_2(n)$ is given by

$$S_2(n) = \sum_{j=1}^{n-1} \frac{(-1)^{j+1}}{\sin^2\left(\frac{j\pi}{2n}\right)}$$
$$= \frac{4n^2}{\pi^2}\sum_{j=1}^{n-1}\sum_{k=0}^{\infty}\frac{(-1)^{j+1}}{(j-2nk)^2} + \frac{(-1)^{j+1}}{[-j-2n(k-1)]^2}$$
$$= \begin{cases} \frac{4n^2}{\pi^2}\sum_{s=1}^{\infty}\frac{(-1)^{s+1}}{s^2} + \frac{1}{(sn)^2} = \frac{n^2+2}{3}, & n \text{ is even} \\ \frac{4n^2}{\pi^2}\sum_{s=1}^{\infty}\frac{(-1)^{s+1}}{s^2} - \frac{(-1)^{j+1}}{(sn)^2} = \frac{n^2-1}{3}, & n \text{ is odd} \end{cases}$$
$$= \frac{n^2-1}{3} + \frac{1+(-1)^n}{2}. \tag{C7}$$

Inserting Eqs. (C6) and (C7) into Eq. (C2), we find that

$$G(\mu_1) \simeq G(0)\left(1 - \mu_1 \frac{u^2+v^2-2}{3}\right),$$

$$h_1(\mu_1) \simeq 2 - \frac{u+v}{uv} + \mu_1\left(\frac{2u^2-3u+1}{3u} + \frac{2v^2-3v+1}{3v}\right),$$

$$h_2(\mu_1) \simeq \frac{u+v}{uv} + \mu_1\left(\frac{u^2-1}{3u} + \frac{v^2-1}{3v}\right). \tag{C8}$$

[1] B. D. Hughes, *Random Walks and Random Environments* (Oxford University Press, Clarendon, 1995), Vol. 1.
[2] D. ben-Avraham and S. Havlin, *Diffusion and Reactions in Fractals and Disordered Systems* (Cambridge University Press, Cambridge, England, 2000).
[3] S. Redner, *A Guide to First-Passage Processes* (Cambridge University Press, Cambridge, England, 2001).
[4] R. Albert and A.-L. Barabási, Rev. Mod. Phys. **74**, 47 (2002).
[5] S. N. Dorogovtsev and J. F. F. Mendes, Adv. Phys. **51**, 1079 (2002).
[6] M. E. J. Newman, SIAM Rev. **45**, 167 (2003).
[7] S. Bilke and C. Peterson, Phys. Rev. E **64**, 036106 (2001).
[8] J. D. Noh and H. Rieger, Phys. Rev. Lett. **92**, 118701 (2004).
[9] N. Masuda and N. Konno, Phys. Rev. E **69**, 066113 (2004).
[10] V. Sood, S. Redner, and D. ben-Avraham, J. Phys. A **38**, 109 (2005).
[11] E. M. Bollt and D. ben-Avraham, New J. Phys. **7**, 26 (2005).
[12] S. Condamin, O. Bénichou, V. Tejedor, R. Voituriez, and J. Klafter, Nature (London) **450**, 77 (2007).
[13] A. Baronchelli, M. Catanzaro, and R. Pastor-Satorras, Phys. Rev. E **78**, 011114 (2008).
[14] Z. Zhang, Y. Qi, S. Zhou, W. Xie, and J. Guan, Phys. Rev. E **79**, 021127 (2009).
[15] V. Tejedor, O. Bénichou, and R. Voituriez, Phys. Rev. E **80**, 065104(R) (2009).
[16] D.-H. Kim, J.-D. Noh, and H. Jeong, Phys. Rev. E **70**, 046126 (2004).
[17] K.-I. Goh, G. Salvi, B. Kahng, and D. Kim, Phys. Rev. Lett. **96**, 018701 (2006).
[18] Z. Wu, L. A. Braunstein, S. Havlin, and H. E. Stanley, Phys.

Rev. Lett. **96**, 148702 (2006).
[19] H. D. Rozenfeld, C. Song, and H. A. Makse, Phys. Rev. Lett. **104**, 025701 (2010).
[20] D. Kim, J. Korean Phys. Soc. **17**, 3 (1984); R. Burioni and D. Cassi, Phys. Rev. Lett. **76**, 1091 (1996); K. Hattori, T. Hattori, and H. Watanabe, Prog. Theor. Phys. Suppl. **92**, 108 (1987).
[21] A. N. Berker and S. Ostlund, J. Phys. C **12**, 4961 (1979).
[22] M. Hinczewski and A. N. Berker, Phys. Rev. E **73**, 066126 (2006).
[23] H. D. Rozenfeld, S. Havlin, and D. ben-Avraham, New J. Phys. **9**, 175 (2007).
[24] H. D. Rozenfeld and D. ben-Avraham, Phys. Rev. E **75**, 061102 (2007).
[25] J. D. Noh and H. Rieger, Phys. Rev. E **66**, 066127 (2002).
[26] C. Song, S. Havlin, and H. A. Makse, Nature (London) **433**, 392 (2005); Nat. Phys. **2**, 275 (2006).
[27] In Ref. [22], Eq. (3) was analytically derived for $u=v=2$ and $p=0$. Also our numerical computation of the mean distance using the link cost $c_{\ell q}=1/W_{\ell q}$ confirms the logarithmic scaling of the mean distance in the WF networks with $p>0$.
[28] The eigenvalues of L are distributed between 0 and 2 as stated in the Perron-Frobenius theorem.
[29] Z. Zhang, Y. Qi, S. Zhou, S. Gao, and J. Guan, Phys. Rev. E **81**, 016114 (2010).
[30] D. Kim and B. Kahng, Chaos **17**, 026115 (2007); G. J. Rodgers and A. J. Bray, Phys. Rev. B **37**, 3557 (1988).
[31] A. N. Samukhin, S. N. Dorogovtsev, and J. F. F. Mendes, Phys. Rev. E **77**, 036115 (2008).
[32] J. Cardy, *Scaling and Renormalization in Statistical Physics* (Cambridge University Press, Cambridge, England, 1996).
[33] J.-D. Han *et al.*, Nature (London) **430**, 88 (2004).
[34] Database of Interacting Proteins, http://dip.doe-mbi.ucla.edu/dip/
[35] M. E. J. Newman, Proc. Natl. Acad. Sci. U.S.A. **98**, 404 (2001).
[36] University of Oregon Route Views Archive Project, http://archive.routeviews.org/
[37] J. S. Kim, K.-I. Goh, G. Salvi, E. Oh, B. Kahng, and D. Kim, Phys. Rev. E **75**, 016110 (2007).
[38] S. Hwang, D.-S. Lee, B. Kahng, and D. Kim (unpublished).
[39] S. S. Cheng, *Partial Difference Equations* (Taylor & Francis, London, 2003).